



# Design, Fabrication, and Application of Micro-Structured Surfaces for Laser-Induced Breakdown Spectroscopic Analysis of Liquids: A Sample-Loading Target Development Studies

Dilara Kaplan, Nadir Aras, Şerife Yalçın\*

İzmir Institute of Technology, Faculty of Science, Chemistry Department, 35430 İzmir, Turkey

## ARTICLE INFO

### Keywords:

Micro-structured surfaces  
Sample-loading target  
Dried-droplet analysis  
Laser-induced breakdown spectroscopy

## ABSTRACT

In this paper, design, fabrication, and application studies of a sample loading target patterned with periodical micro-structures were presented. Two different geometrical shapes; triangular prisms and cylinders of two different feature sizes; 5- $\mu\text{m}$ , and 20- $\mu\text{m}$ , were photo-lithographically patterned on Si-wafer substrates, and dry etched to 10  $\mu\text{m}$  height. Followed by a 1- $\mu\text{m}$  thick silicon nitride film coating over micro-patterned substrates, final products were obtained after dicing into one-inch size squares, each containing 36 patterned sample loading areas. Among the three different patterns studied; a geometric design with 20- $\mu\text{m}$  diameter cylinders exhibited a more effective task in increasing the LIBS signal strength, compared to the other two patterns. The characterization of the surface morphology and the size-shape distribution of the micro-patterns were carried out through optical and scanning electron microscopic measurements. SEM images proved a more effective ablation occurring on triangular prism micro-structured surfaces that can be associated with an increased path length and enhanced absorption of the laser beam on the flat surfaces of triangular prism via multiple reflections. The results of structured surfaces were also compared with the ones from non-structured surfaces of 300 nm and 1000 nm thicknesses of silicon nitride-coating. The applications of micro-structured surfaces for heavy metals analysis were performed with Cr and Pb solutions via dried-droplet LIBS methodology. The enhancement factor of 4 for Pb(I) 405.8 nm, and 8 for Cr(I) 428.9 nm were observed from the 20- $\mu\text{m}$  diameter cylinder, CYL-20, surfaces compared to 300 nm thick  $\text{Si}_3\text{N}_4$  surfaces, respectively. This study of micro-structuring substrate surfaces with an emphasis on the signal enhancement effect is promising in terms of improving the capacity and limitations of the dried-droplet methodology by LIBS.

## 1. Introduction

Some material properties insignificant at the macro-scale become important at the micro- and nanoscale, and the performance of the products increases. Therefore, the production of very small devices or features in micrometer/nanometer precision, Micro/Nano-Machining [1,2], has become the center of attention in science and industry. A variety of micromachining technologies, like photolithography, wet/dry etching, and thin-film deposition are developing to serve the needs of scientists and engineers in research and industries [3–7]. Laser-induced structuring [8], in which ultrashort laser pulses are used for the formation of periodic patterns on the surface, is an appealing alternative to commonly used microfabrication techniques, although the optical diffraction limit and the size of the heat-affected zone are the main

limitations in the production of extremely small features. Materials used in micromachining technology include glass, polymers, metals, and alloys, however, the silicon wafer is the most widely used substrate material in many manufacturing technologies.

Laser Induced Breakdown Spectroscopy, LIBS [9] is an analytical technique that uses focused laser pulses to create a micro-plasma for the determination of elemental compositions of all types of samples in solid, liquid, and gaseous form, in-situ and in real-time. Compared to solid and gaseous samples, direct-liquid analysis by LIBS has some drawbacks. Splashing, bubbling, and evaporation are some of the obstacles faced in direct-liquids analysis by LIBS, which result in plasma instability, quenching, and low analytical performance. To solve these problems encountered, various chemical approaches and methodologies were explored [10,11]. Among them, the conversion of the sample from liquid

\* Corresponding author.

E-mail address: [serifeyalcin@iyte.edu.tr](mailto:serifeyalcin@iyte.edu.tr) (Ş. Yalçın).

<https://doi.org/10.1016/j.microc.2023.109568>

Received 19 September 2023; Received in revised form 16 October 2023; Accepted 26 October 2023

Available online 31 October 2023

0026-265X/© 2023 Elsevier B.V. All rights reserved.

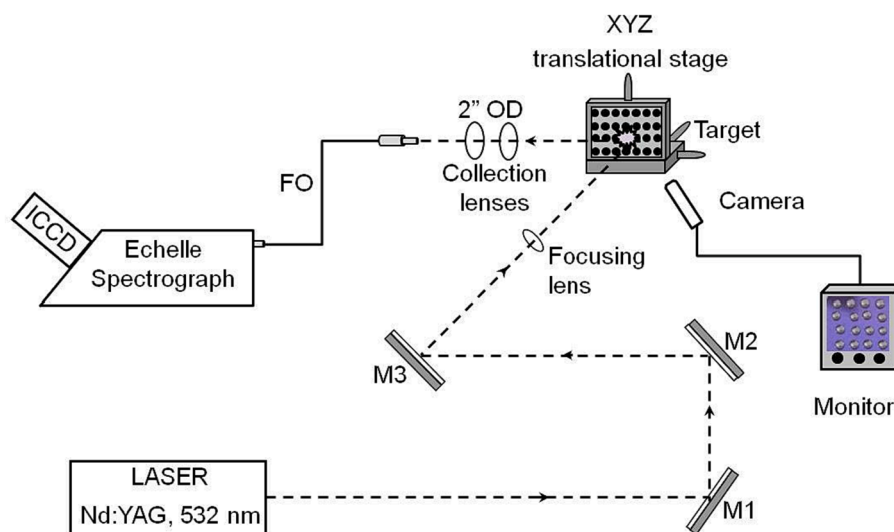


Fig. 1. Experimental LIBS setup. M1, M2, and M3: reflecting laser mirrors, FO: fiber optic cable, ICCD: Intensified Charge Coupled Detector.

to solid phase before analysis provides a higher detection sensitivity as the stability of the analyte in the sampling region is achieved. Conversion of the liquid sample into a solid form can be established by simply applying the sample on **absorbent surfaces** like, membrane-based filter paper [12], wood slice [13], polymer fiber [14], graphene oxide [15], or on **non-absorbent surfaces** like metals [16,17]. Metal surfaces like Al, Zn, Mg, and Ni are actively used in the scope of Surface Enhanced Laser Induced Breakdown Spectroscopy research, SENLIBS, in which enhancement in signal strength and increase in the detection power of the LIBS technique is obtained from the plasma created by the interactions of laser pulses with sample and metallic substrate. However, there are a few reports in the literature based on the use of **non-metallic substrates** for SENLIBS research [18–20]. Bae et al. [18] used a laser-patterned silicon wafer (LPSW) substrate to spread the water and found the average relative standard deviation (RSD) of potassium measurements was lower than 6 %. In another study, a porous silicon substrate in the presence of gold nanoparticles [19] was used to investigate the position-to-position signal strength of the emission signal from dried droplets. 10 % RSD of the Strontium signal from 15 laser shots on a porous Si substrate was reported. The use of gold nanoparticles on silicon nitride substrate [20] enabled heavy metal ions Cu, Pb, and Cr detection with LODs of  $5 \text{ ng mL}^{-1}$ ,  $22 \text{ ng mL}^{-1}$ , and  $9 \text{ ng mL}^{-1}$ , respectively.

We have been studying, for almost a decade, the effect of using Si-wafer-based non-metallic substrates on laser-induced breakdown spectroscopic signal strength, in liquids analysis via dried-droplet methodology [21–23]. In one of our studies, enhancements in the signal strength of several elements were obtained with the use of 300 nm oxide-coated Si-wafer substrates ( $\text{Si} + \text{SiO}_2$ ). Absolute amounts of 1.26 pg Cu, 3.32 pg Mn, 79 pg Cd, and 47.6 pg Pb were detected with this methodology. In another study, the analytical performance of the three Si-wafer-based substrates: pure silicon wafer, 300 nm silicon oxide coated Si-wafer, and 300 nm silicon nitride coated silicon wafer were comparatively studied. It has been observed that silicon nitride-coated Si-wafer substrates enhanced the LIBS signal intensity the most, compared to that of  $\text{SiO}_2$ -coated and c-Si wafer substrates, for all elements studied, Cd, Cr, Cu, Mn, and Pb. Silicon nitride films, due to antireflective properties, provide higher photon transmission and significant absorption of the laser beam on the surface where the energy is effectively transferred to the analyte residues of the dried droplets. Recently, the effect of silicon nitride coating thickness for enhanced sensitivity in the dried-droplet LIBS analysis was studied [23]. Among the substrates of different nitride coating thicknesses (75, 300, 450, and 1000 nm), a substrate with 1000 nm thick nitride coating has shown the

most significant improvement in signal strength of the Pb, Cu, and Cr elements.

To further investigate the effect of surface topography on the efficiency of LIBS detection, micro-patterning of the Si-wafer surfaces was aimed. It is well known that the micro-structuring of silicon wafer surfaces plays an important role in improving the performance of technological products such as solar cells, sensors, and imaging devices in MEMS applications [24]. Photons interacting with micro-structured surfaces provide high sensitivity, due to increased surface area up to 2–1000 times [25].

In this paper, micro-structuring Si-wafer surfaces for signal enhancement and hence improvement in the analytical capability of the LIBS technique for dried-droplet methodology is presented. For this purpose, design, construction, and application studies were performed. Geometrical patterns in different sizes and shapes (5- $\mu\text{m}$  diameter cylinder, 20- $\mu\text{m}$  diameter cylinder, and 5- $\mu\text{m}$  side length triangular prism) were designed and photo-lithographically printed on c-Si wafer substrates. These microstructures were then etched to 10- $\mu\text{m}$  height by dry etching method and then coated with a 1- $\mu\text{m}$  thick antireflective  $\text{Si}_3\text{N}_4$  layer by plasma chemical vapor deposition process. The fabricated products were diced into one-inch squares, each containing 36 patterned sample loading areas. 500 nl of aqueous heavy metal solutions were loaded on these micro-structured spots and analyzed by LIBS after drying. The application studies of micro-structured surfaces for Laser-Induced Breakdown Spectroscopic analysis of heavy metals were carried out with aqueous solutions of Cr and Pb. Results obtained from the micro-structured surfaces were compared with the ones from non-structured  $\text{Si}_3\text{N}_4$  surfaces.

## 2. Experimental

In this section, the steps in the production of micro-structured Si-wafers, the instrumental LIBS setup, the sampling methodology, and the chemicals used in this study will be explained.

### 2.1. The steps in Micro-Structuring Si-wafer surfaces

Microstructures on Si-wafer surfaces are facilitated through the use of several leading-edge technologies and the processes generally consist of three basic steps; pattern printing, surface etching, and thin-film coating. However, before printing the patterns on a substrate, the geometric patterns had to be selected, designed, and drawn with suitable software. In this study, the geometrical patterns were drawn in **AutoCAD** format. After the pattern design studies were performed, the

**Table 1**  
Optimum experimental LIBS conditions.

Element	Laser pulse energy (mJ)	Delay time, ( $T_d$ )	Gate time, ( $T_g$ )
Cr (428.9 nm)	135	300 ns	100 $\mu$ s
Pb (405.8 nm)	135	2 $\mu$ s	900 $\mu$ s
Cu (324.8 nm)	135	300 ns	1.4 ms

following microfabrication processes; 1) photomask production, 2) pattern transfer from the photomask onto the wafer, 3) etching the structures to a certain depth, 4) thin film coating on the micro-structures, and finally, 5) dicing the Si-wafer substrate for the separation of many sample loading targets, were performed. These high-technology processes were performed through a company **Rose Fotomasken, Germany**.

Initially, a photomask was produced from 6x6 inch soda lime glass, and microstructures from the photomask were photo-lithographically printed onto the 5" diameter Si-wafers. Photo-lithography [26], also known as optical lithography, is a technique in which UV light is used to transfer shapes from a mask onto a silicon substrate. For this, the wafers were coated with a photosensitive material, photoresist, and then the photomask was placed between a light source and the Si-wafer. The photoresist reacts to the light and the resultant pattern was developed. These microstructures were then etched to 10- $\mu$ m height, via deep reactive ion etching, DRIE, process. DRIE is a widely available technique used to etch deep trenches and has a very high etch selectivity for silicon. After etching to 10  $\mu$ m deep, a 1- $\mu$ m thick silicon nitride film was coated over these micro-structures by Plasma Chemical Vapor Deposition Process, PCVD. Each different pattern region was diced into 1-inch squares to be used as a final product, a sample loading target.

Further details on the design, production, and application studies of the micro-structured products are given in the results section.

## 2.2. Instrumental LIBS setup

The LIBS setup used in this study, given in Fig. 1. consisted of a Nd:YAG laser source (*Quanta-Ray Lab-170, Spectra-Physics*) with 10 ns pulse

duration, operating at its second harmonics, 532 nm wavelength.

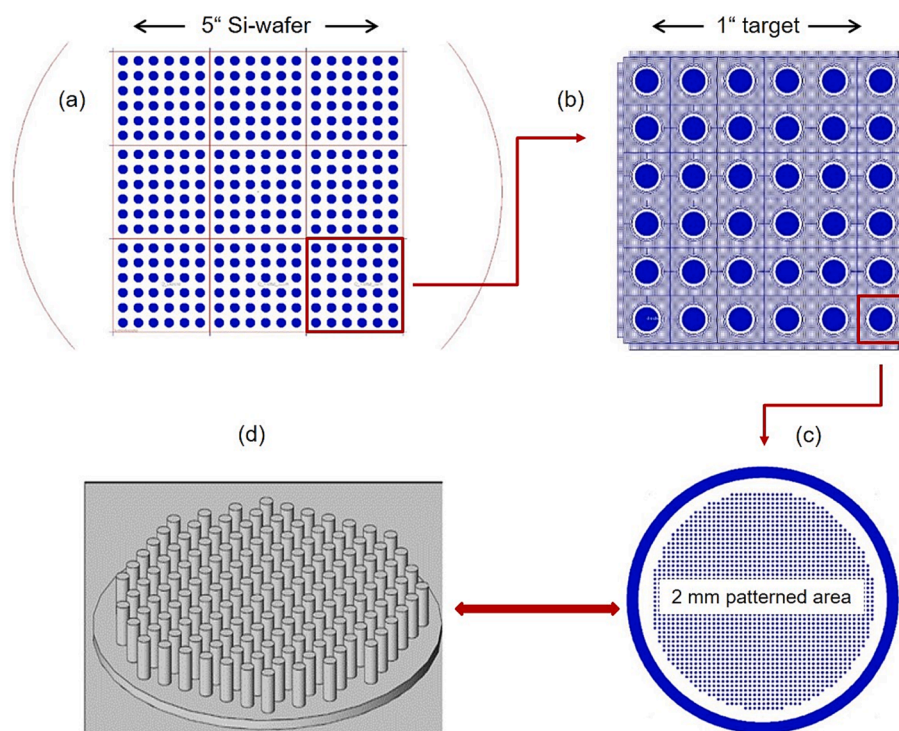
A 17.5 cm focal length lens is positioned a few cm in front of the minimum focal point to ensure the diameter of the laser beam is about the same as the droplet size. The optical geometry used in this study focuses the laser beam to a relatively large spot therefore, higher laser pulse energies are required for ablation [21,22]. Laser beams with an optimum pulse energy of 130 mJ are sent onto the micro-structured substrate surfaces where dried-droplet samples are located. The resulting plasma emission is collected with suitable lenses and directed onto the entrance slit of a spectrograph (Mechelle 5000, Andor Inc.) by a fiber optic cable and analyzed by an ICCD detector (iStar DH734, Andor Inc.). The spectral range of the Spectrograph is 200–850 nm and the resolution is 0.08 nm at 400 nm wavelength. A vision camera and a monitor system were used for the observation of the dried droplets before and after ablation to decide on the sampling position.

To maximize analyte signal intensity, optimization of instrumental LIBS parameters like detector delay time, gate width, and laser pulse energy has been performed for each element, separately, according to the procedure described elsewhere [21], Table 1. given below, lists the optimum experimental conditions for each element at its prominent emission wavelength. All spectra are obtained from the accumulation of 3 to 5 single laser pulses on the same spot and an average signal from 3 to 5 separate droplets was used for quantification. The measurements were performed with > 80 % accuracy and 10–15 % precision.

## 2.3. Reagents, Chemicals, and sampling methodology

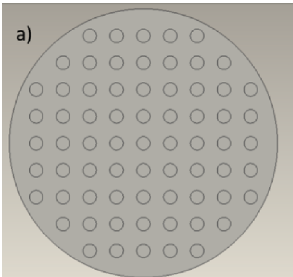
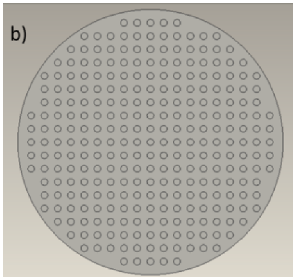
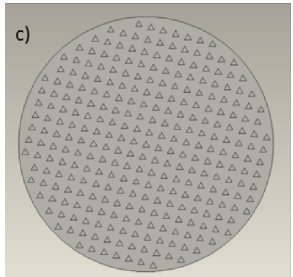
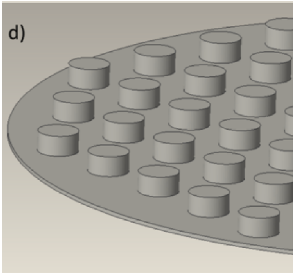
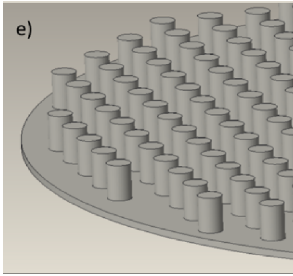
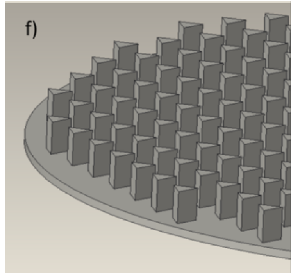
Single-element standard solutions of heavy metals (*High-Purity Standards*), 1000 mg L<sup>-1</sup>, were used by suitable dilution with ultrapure water. Si-wafers with 300 nm and 1000 nm thick silicon-nitride coating (*Microchemicals GmbH*) were used with no treatment.

Heavy metal solutions were analyzed via the dried-droplet methodology consisting of loading, drying, and analysis steps. In this methodology, 500 nl volumes of aqueous solutions are manually deposited on 2 mm diameter micro-structured sample-loading spots. After approximately 5 min of drying at room temperature, the substrate containing dried-droplet residue is located on the sample holder apparatus, and



**Fig. 2.** Top-to-bottom graphical representation of the sample loading target design made in AutoCAD software.

**Table 2**  
Micro-pattern design and size selection.

Mask Pattern			
Wafer Pattern			
Pattern dimensions	<i>Cylinder</i> r = 10 $\mu\text{m}$ h = 10 $\mu\text{m}$	<i>Cylinder</i> r = 2.5 $\mu\text{m}$ h = 10 $\mu\text{m}$	<i>Triangular prism</i> a = 5 $\mu\text{m}$ h = 10 $\mu\text{m}$
- # of the patterns	- 1917	- 31,233	- 31,248
- surface area	- 4.35 $\text{mm}^2$	- 8.05 $\text{mm}^2$	- 7.83 $\text{mm}^2$

analyzed by high-energy laser pulses of approximately 1.5 GW/cm<sup>2</sup> power density. A translational stage, on which a sample loading target is attached, is used to change the sampling position manually for a fresh spot.

### 3. Results and discussion

To find a solution to the inhomogeneous distribution problem of the liquid droplets on the Si-wafer substrates and provide enhancement in the LIBS signal strength, design, fabrication, and application studies to heavy metals analysis were performed.

#### 3.1. Micro-pattern design studies

In this part, the selection, design, and drawing studies of the micro-patterns to be printed on the Si-wafer substrate are presented.

The diameter of the circular area occupied by the 500 nL of aqueous droplet on a substrate surface is about 1.5 mm therefore, the size of each sample loading area to be micro-patterned was selected to be as large as 2 mm in diameter. The distance between the two sample loading areas was also kept at 2 mm apart by considering possible contamination of the sample loading area by the material sputtered out from the previous sampling, due to surface explosion and shock wave expansion. As is shown in the top-to-bottom graphical representation of the sample loading target design, in Fig. 2., with the use of a 5-inch diameter Si-wafer substrate, there would be nine sample loading targets produced. Each target is 1-inch square in size, Fig. 2(a), and within each 1-inch square target, there would be 6x6 = 36 sample loading spots each with 2 mm diameter and 2 mm spacing in between, Fig. 2(b). Inside each

of these sample loading spots, patterns of cylinders and triangular prisms are designed, Fig. 2(c, d). The pattern's geometric shape and size selection in these 2 mm diameter circular areas was made to emphasize the effect of surface area on LIBS signal strength. Therefore, the sampling areas of 2 mm diameter circles were patterned with two different geometric shapes (cylinder and triangular prism), and two different sizes of the same geometric shape (small cylinder-5  $\mu\text{m}$  and large cylinder-20  $\mu\text{m}$  in diameter).

The height of each pattern was selected to be 10  $\mu\text{m}$  and the spacing between geometric patterns is designed to be the same as the micro-structure size. This way, the shape and size effect on the LIBS signal strength would be investigated. The shape of the patterns on the mask and on the wafer, drawn with AutoCAD software, and the corresponding number of the patterns and their surface area by calculation, are given in Table 2.

The number of patterns that can fit into a 2-mm diameter circular area from 5- $\mu\text{m}$  diameter cylinders and 5- $\mu\text{m}$  side length triangular prisms are close to each other, being 31,233 and 31,248 patterns, respectively. Also, there is not much difference in the surface area of the patterns with these geometrical shapes, being 7.83  $\text{mm}^2$  and 8.04  $\text{mm}^2$ , respectively. On the other hand, the number of patterns with 20- $\mu\text{m}$  diameter cylinders in a 2-mm diameter sampling area is 1917, and the corresponding surface area from these patterns is 4.35  $\text{mm}^2$ . As the feature size gets larger, the surface area gets smaller, as expected. Patterns with 20- $\mu\text{m}$  diameter cylinders have a smaller surface area and a smaller number of patterns compared to those of the other two patterns.



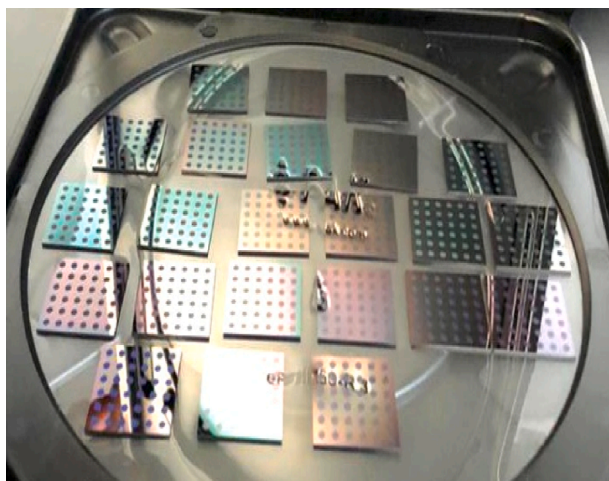


Fig. 3. A picture of 1-inch-square micro-structured Si-wafer targets was produced.

### 3.2. Fabrication studies of a sample loading target and investigations of surface topographies

The patterns designed in AutoCAD software were lithographically printed onto the 5-inch diameter and 625- $\mu\text{m}$  thick Si-wafer substrates by the use of a photomask. These microstructures were then etched to 10- $\mu\text{m}$  height, via deep reactive ion etching, DRIE, process. Followed by a one-micrometer thick anti-reflective silicon nitride coating on top of the microstructures by the Plasma Chemical Vapor Deposition Process, PCVD, the separation of nine different fields was obtained by dicing the substrate into 1-inch squares. Each 1-inch square Si-wafer target contains a  $6 \times 6 = 36$  sample loading area as can be seen in Fig. 3.

To inspect the fabrication quality of the microstructures produced, the optical microscope images of the micro-patterned surfaces were carried out, first. As is shown in Fig. 4(a), rounding is observed at the corners of the triangular prism design patterns.

A more detailed examination of the micro-structured surfaces was carried out through Scanning Electron Microscope, SEM images given in Fig. 5(a–f). Micro-patterns in a 2-mm sample loading area and a 10- $\mu\text{m}$  high barrier frame around this area can be seen in Fig. 5(a). This 10- $\mu\text{m}$  high barrier frame around the sample loading area is designed to prevent liquid samples from flowing into the next sampling area. SEM images of micro-patterns with 20- $\mu\text{m}$  and 5- $\mu\text{m}$  diameter cylinders and 5  $\mu\text{m}$  side-length triangular prisms are given in Fig. 5(b–d), respectively. The rounding at the corners of triangular patterns, observed in optical microscope images as well, appears more clearly and is related to the limitations in the resolution of the fabrication system. The SEM image of some accidentally damaged patterns at the edge of the sample loading area, Fig. 5(e), allowed us to obtain the pattern height information. A cylinder height of 11.4- $\mu\text{m}$ , as is seen in the zoomed-in image in Fig. 5(f),

indicates success in pattern fabrication, considering a 1- $\mu\text{m}$  thick anti-reflective nitride coating is applied on 10  $\mu\text{m}$  high micro-structured surfaces with  $\pm 2\text{-}\mu\text{m}$  tolerance. It is also observed that the diameters of the cylinders at the top are larger than the bottom diameters corresponding to a  $\pm 1\text{-degree}$  deviation angle for the DRIE-Bosh process applied during fabrication.

Another point that should be considered about the fabricated products is the spatial variation in the antireflective coating thickness. In thin film coating processes, it is known that the coating is denser on the hills than the ones on the bottom. Therefore, Si-nitride coating thickness is expected to be less on the bottom between the features, than the ones on top of the structures, which results in variations in coating density in the production process. A more careful look at the top-right corner of Fig. 5 (f), one can notice the “undulations” or “ripples” on the sidewalls of the cylinders, which are due to the cyclic nature of the Bosch DRIE process. The technique is not preferred for the construction of nanostructures, due to in-tolerable sidewall-rippling on the nanoscale.

### 3.3. Applications of the micro-structured surfaces for heavy metals analyses by LIBS

The application studies of micro-structured surfaces for Laser-Induced Breakdown Spectroscopic analysis of heavy metals were carried out with aqueous solutions of Cr and Pb, via dried-droplet methodology. Among the tree designs studied, the most effective micro-structured substrate was determined with an emphasis on analyte signal enhancement. A comparison of the analyte signal strengths from the structured and non-structured surfaces was also performed.

#### 3.3.1. Signal enhancement from the micro-structured surfaces of different sizes and shapes

To study the effect of micro-structures on LIBS signal strength, three substrates patterned with different geometries and sizes were used. The substrates were named considering the shape and size of the micro-patterns on them. The substrates patterned with cylinders of 5- $\mu\text{m}$  and 20- $\mu\text{m}$  diameters are named CYL-5 and CYL-20, respectively, while substrates patterned with triangular prisms of 5- $\mu\text{m}$  side length are named TAP-5. Fig. 6. shows the variations in the LIBS signal strength with respect to pattern geometry and size of the substrates for emission lines of the Cr and Pb, within the spectral region that represents the most probable transitions. It is observed that the analyte signal obtained from the CYL-5 substrate surfaces is stronger than the one obtained from the TAP-5 substrate surface. Also, the LIBS signal observed from the CYL-20 substrate surface is much stronger than that of the other two. The order of signal enhancement is TAP-5, CYL-5, and CYL-20, for both Cr and Pb emission lines. This order of signal enhancement is unexpected.

The initial motivation of this study in patterning the Si-wafer surfaces with microstructures was to increase the surface area that the laser light can interact and thus more efficient atomization and plasma formation through enhanced absorption is provided. Therefore, signal intensity from the substrates patterned with smaller micro-structures

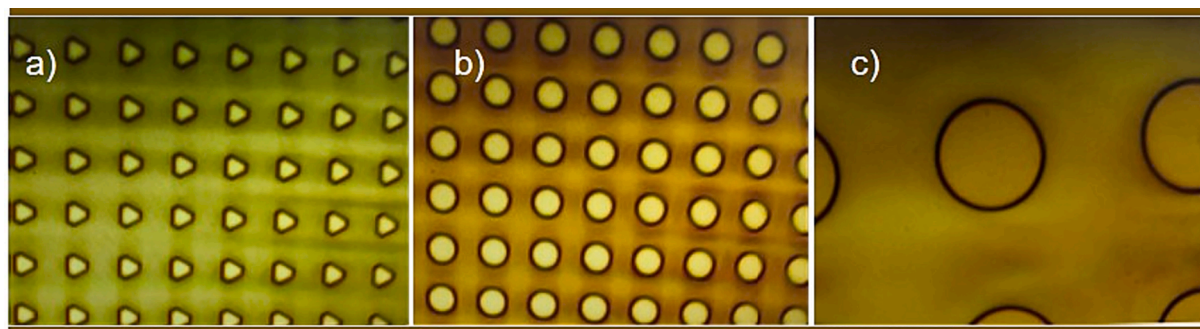


Fig. 4. Optical microscope images of the (a) 5- $\mu\text{m}$  side length triangular prism, (b) 5- $\mu\text{m}$  diameter cylinder, and (c) 20- $\mu\text{m}$  diameter cylinder.

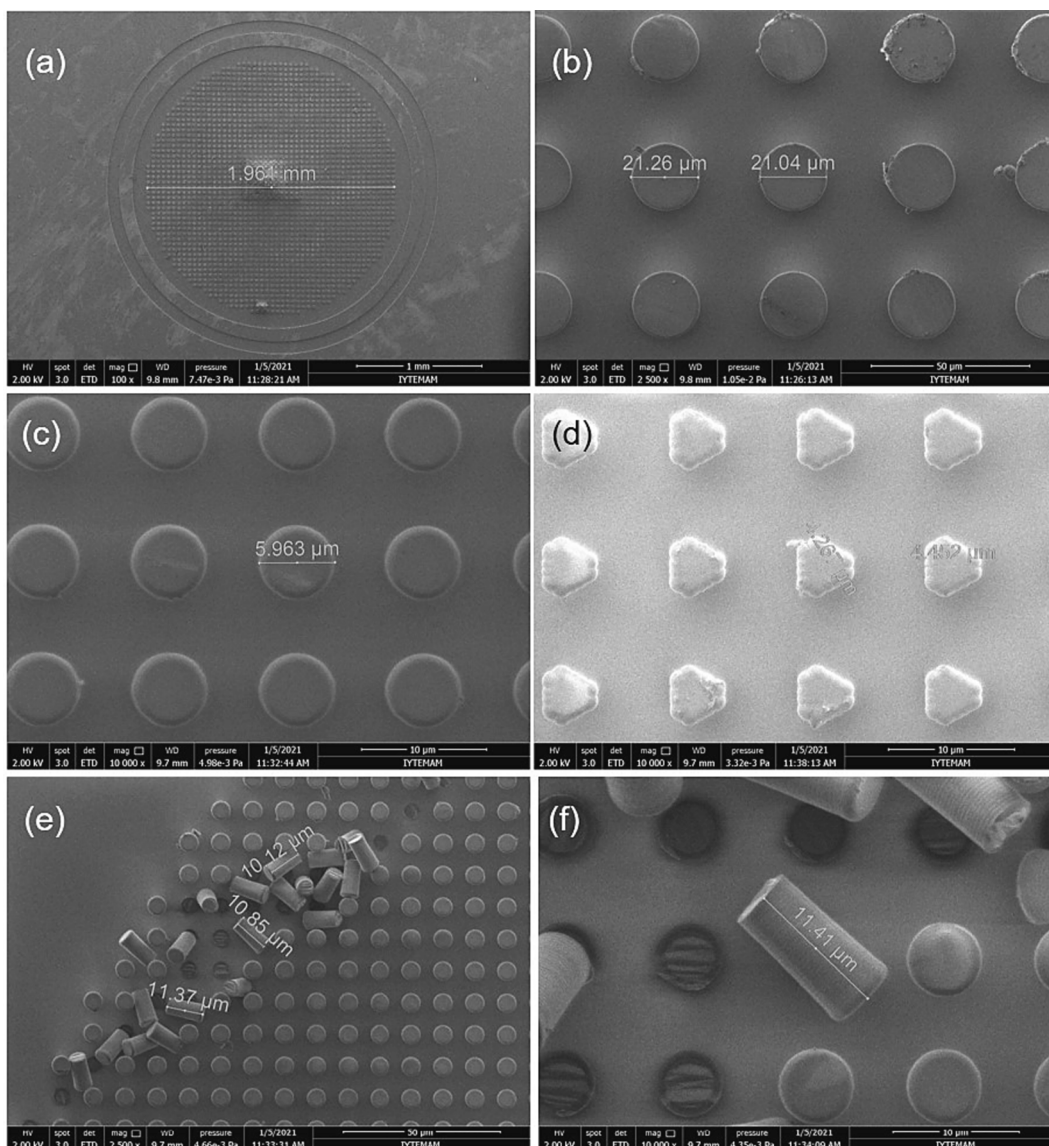


Fig. 5. Scanning Electron Microscope (SEM) images of the micro-structured surfaces. (a) 2 mm diameter sample loading area, (b) 20-µm diameter cylinders (mag:2500), (c) 5-µm diameter cylinders (mag:10000), (d) 5-µm side length triangular prisms (mag:10000), (e-f) height information from the damaged region.

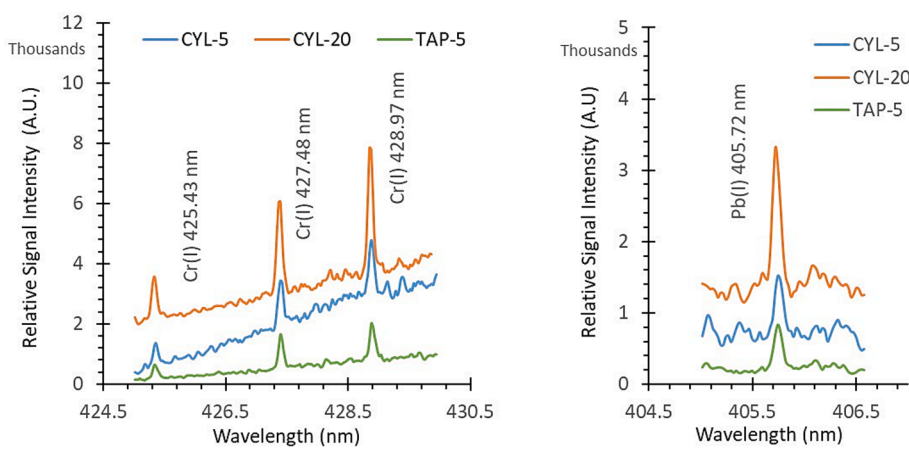
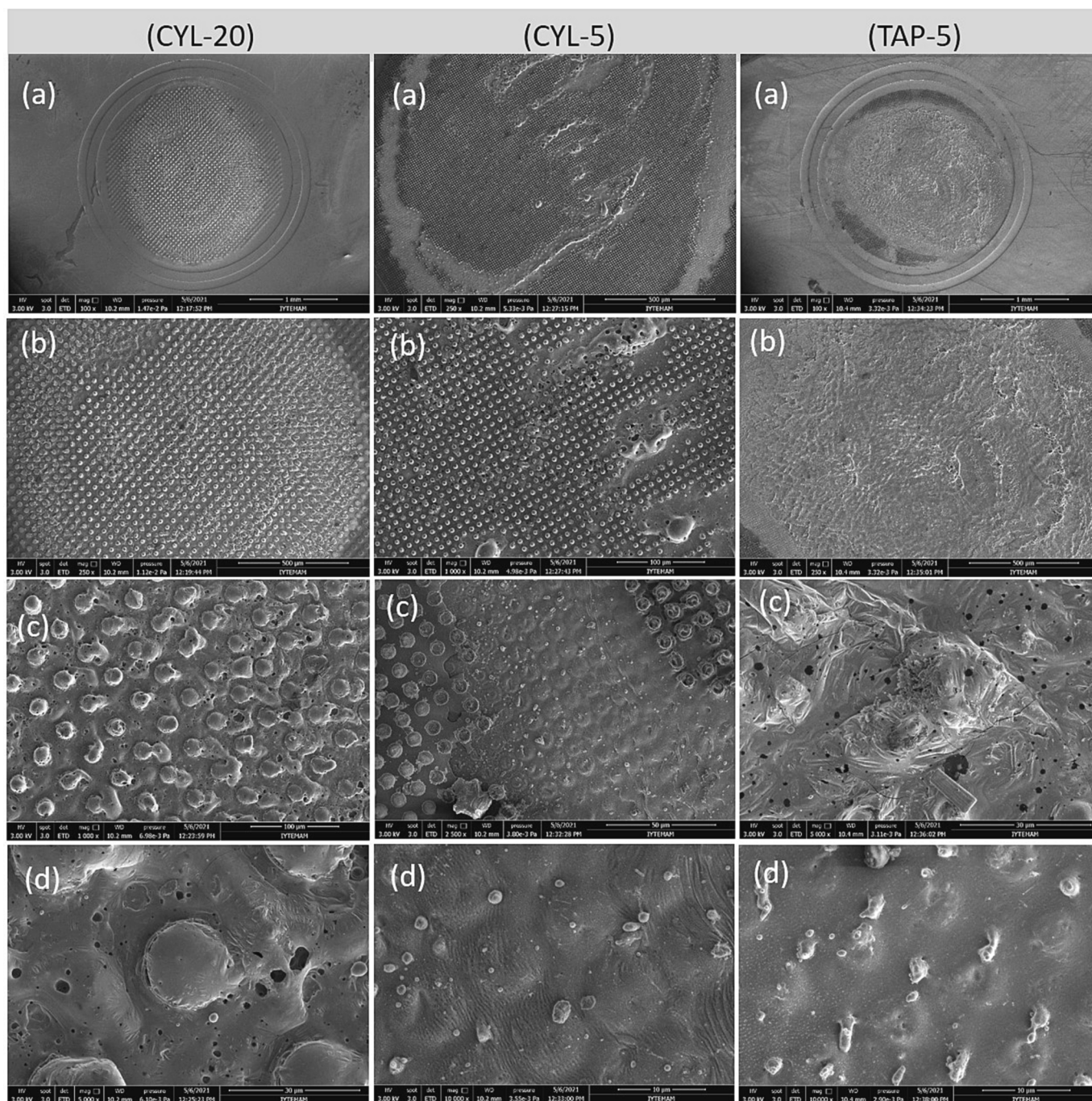


Fig. 6. Variations in relative signal strength of Cr and Pb on three micro-structured substrate surfaces at their optimum experimental conditions.





**Fig. 7.** SEM images of laser-ablated substrate surfaces from left to right in series: CYL-20, CYL-5, and TAP-5. Enlarged viewing of the craters from top to bottom, (a-d), for each substrate type.

(CYL-5 and TAP-5) of about  $8 \text{ mm}^2$  surface area would be expected to be higher than that of CYL-20 one with  $4.35 \text{ mm}^2$  surface area. However, this is not the case.

To better understand why larger cylinders with a smaller aspect ratio (*height to width ratio of the microstructures*) improve LIBS signal strength more than that of the smaller size structures with larger aspect ratio, SEM images of the substrates after ablation were inspected. Full images of the laser-ablated craters are given in Fig. 7(a) of each substrate type, CYL-20, CYL-5, and TAP-5. Enlarged viewings of the ablated spots given from top to bottom, (a-d), in Fig. 7 help us to understand the physical aspects of the phenomenon observed.

In general, the extent of the damage is not the same throughout the craters. For each substrate, it is more in some parts of the craters and less

in the remaining parts due to the inhomogeneity in the spatial distribution of the laser pulse energy. Apart from that, when the extent of the damage is compared from one substrate to another, more destructive damages are observed on the TAP-5 surfaces than the ones on the other substrates, CYL-20 and CYL-5. It is observed that the triangular prism microstructures disappeared, and the melted material spread towards the edges with shock wave expansion, as is shown in (TAP-5-b). Cracking, hole formation due to boiling, shrinkage, and wrinkle formation with cooling can be seen in (TAP-5-c). The scattered and fallen-down structures as a result of melting in the crater area are observed as shown in (TAP-5-d). The deformations on the CYL-5 substrate surfaces are higher than the CYL-20 substrate and lower than that of the TAP-5 ones. The circular spots of  $5\text{-}\mu\text{m}$  diameter cylinders are apparent,

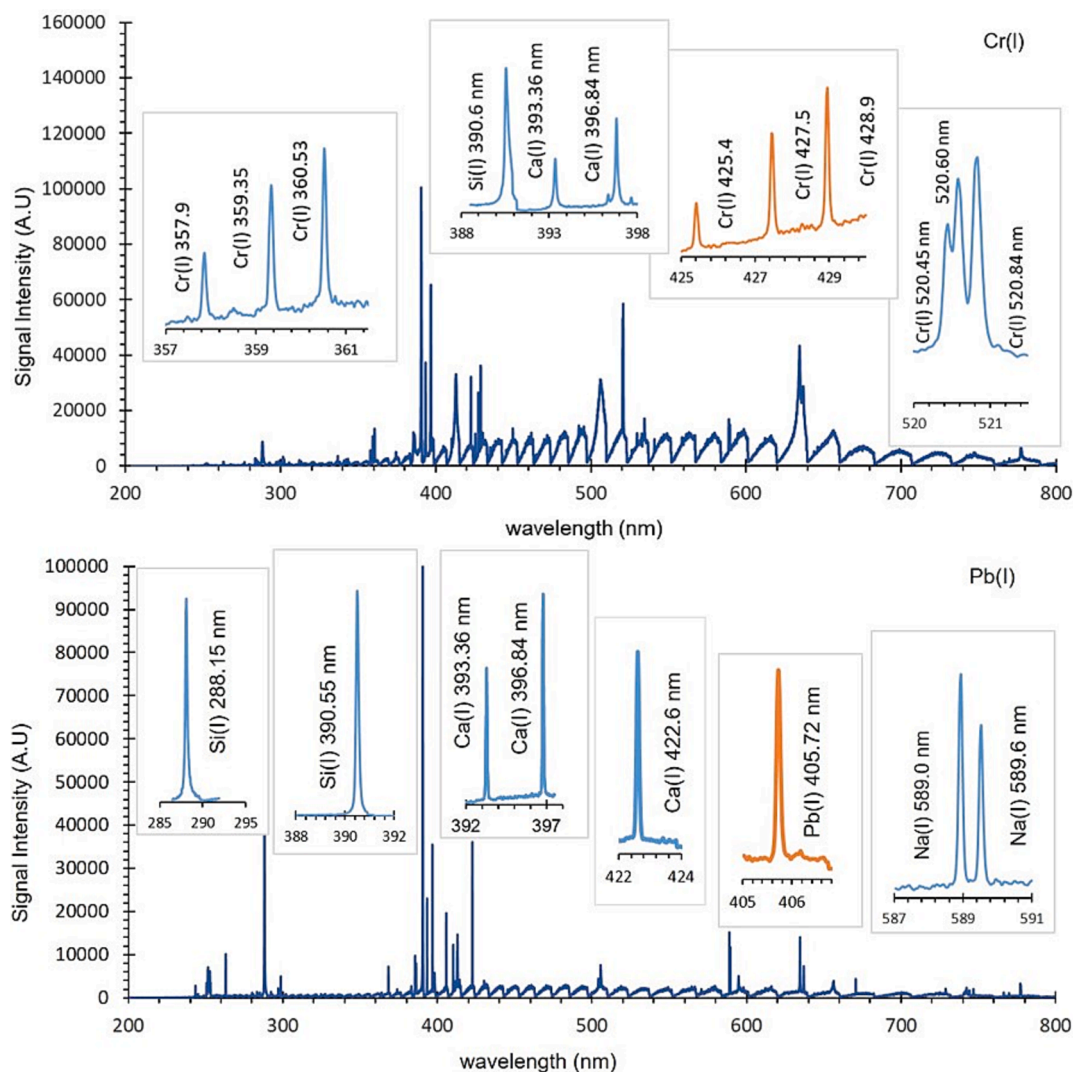


**Fig. 8.** Representative LIBS spectra from the dried droplets of Cr, and Pb solutions on CYL-20 substrate surface. Spectra are from the single deposition of 100  $\mu\text{g/L}$  metal solutions.

(CYL-5-d). The melting and boiling behaviors are also observed in CYL-20 substrates, however, unlike TAP-5 surfaces 20- $\mu\text{m}$  diameter cylinders are still standing with some damage. SEM images revealed the fact that the most damaged surface is from TAP-5, then CYL-5, and then CYL-20 substrates. One can claim that; flat side walls of the triangular prism structures, that are interacting with the laser beam, exhibit an enhanced light trapping effect through multiple reflections, and more energetic ablation on TAP-5 structured surfaces is observed. However, the LIBS signal intensity from this TAP-5 surface is the lowest, compared to the other structured surfaces. This reduced signal intensity can be due to the scattering of the plasma emission before reaching the detector by the dust and small particles emerging from the surface after severe ablation. One can also hypothesize that the narrower spacing between 5- $\mu\text{m}$  structures may facilitate more trapping of the plasma emission signal through multiple reflections as opposed to 20- $\mu\text{m}$  ones.

Since CYL-20 substrates exhibit a more effective task in increasing the LIBS signal strength, comparison experiments were performed between CYL-20 and flat substrates.

### 3.3.2. Comparative studies of micro-structured and non-structured surfaces

Full-range LIBS spectra of the Cr and Pb elements between 200 and 800 nm spectral region under optimum experimental conditions are presented in Fig. 8.

Several ionic and neutral emission lines of analyte; Cr and Pb, along with the substrate, Si, and impurity, Na, and Ca, signals are observed. Here, the spectra are from the single deposition of 500 nL of 100  $\mu\text{g/L}$  metal solution, which corresponds to the detection of 50 picogram samples, in absolute amounts, after drying on the CYL-20 substrate. Highly intense signals from the Cr and Pb analytes are promising in terms of the detection limits and analytical figures that could be achieved. Furthermore, pre-concentration of the analyte on the substrate surface through repeated loading and drying procedures in the same sampling spot may provide the detection of even lower concentration solutions. A more comprehensive study, for the establishment of the analytical performance of the micro-structured substrates for quantitative LIBS research, is the subject of another ongoing research in our group.

Our most recent study was on the effect of antireflective  $\text{Si}_3\text{N}_4$  coatings of several thicknesses on the LIBS signal enhancement and it is observed that the silicon wafers with a coating thickness of 1000  $\mu\text{m}$  improve the LIBS signal more than the one with 300 nm coated substrate [23]. Here, in this paper, the signal enhancement effect of micro-structured surfaces followed by nitride-coating was evaluated in comparison with 300 nm and 1000 nm  $\text{Si}_3\text{N}_4$ -coated flat Si-wafer surfaces. For most emission lines of analyte species investigated; Cr(I), typically at 357.9 nm, 359.35 nm, 360.53 nm, 425.4 nm, 427.5 nm, and 428.9 nm,



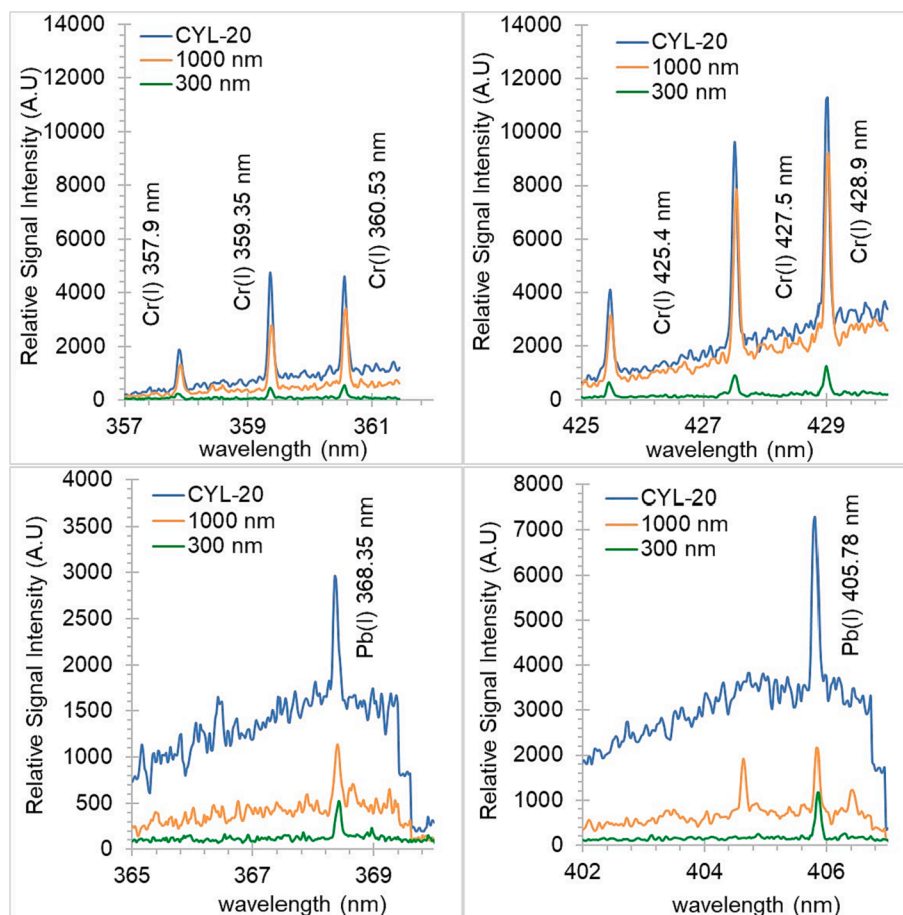


**Fig. 9.** Signal Enhancement Effect observed from the dried droplets of Cr, and Pb solutions on CYL-20 substrate surfaces compared with the ones on 300 nm and 1000 nm silicon nitride coated surfaces. Spectra are obtained from the single deposition of 500 nL of 30  $\mu\text{g/L}$  standard metal solutions.

and Pb(I) at 368.35 nm, and 405.78 nm, structured (CYL-20) surfaces are more sensitive in enhancing the LIBS signal compared to both non-structured, (300 nm and 1000 nm Si<sub>3</sub>N<sub>4</sub> coated) surfaces, as displayed in Fig. 9. In agreement with our previous observations, the LIBS signal from 1000 nm thick Si<sub>3</sub>N<sub>4</sub> coated substrates is significantly higher than the ones obtained on 300 nm Si<sub>3</sub>N<sub>4</sub> coated surfaces. Especially for the element of Pb, there is a significant difference in the intensity of the LIBS signal from the CYL-20 surfaces compared to non-structured ones. The extent of magnitude in the signal enhancement relative to 1000 nm and 300 nm Si<sub>3</sub>N<sub>4</sub> coated substrates was element and emission wavelength specific. For the 405.8 nm emission line of Pb(I), the signals from the CYL-20 substrates were enhanced almost by 3, and 4 times, relative to 1000 nm and 300 nm Si<sub>3</sub>N<sub>4</sub> coated substrates, respectively. When the 428.9 nm Cr(I) line is considered the enhancement from CYL-20 substrate surfaces relative to 1000 nm and 300 nm Si<sub>3</sub>N<sub>4</sub> coated substrates becomes 1.3 and 8 times. The enhancements observed from the CYL-20 surfaces with respect to 300 nm thick Si<sub>3</sub>N<sub>4</sub> surfaces are higher than those for 1000 nm thick Si<sub>3</sub>N<sub>4</sub> coatings. The observed enhancements are from both the presence of micro-structures and the thickness of the anti-reflective layer. However, since all micro-structured surfaces have the same (1000 nm) anti-reflective coatings on top of the structures, the enhancements observed from the comparison of micro-structured substrates and 1000 nm thick Si<sub>3</sub>N<sub>4</sub> coated flat substrates can be associated with the microstructure effects. When the enhancements in micro-structured and 300 nm nitride-coated flat surfaces are considered, both micro-structure and coating thickness effects are taking place, altogether. Therefore, the enhancement factors in comparison with 300 nm Si<sub>3</sub>N<sub>4</sub> surfaces are higher.

#### 4. Conclusions

In this study, the presence of periodic microstructures on the LIBS signal strength has been investigated. For this purpose, Si-wafer substrates with two different geometric shapes (cylinders, and triangular prisms), and two different sizes, (5 nm and 20 nm), were designed and fabricated. One micrometer-thick Si<sub>3</sub>N<sub>4</sub> antireflection layer was coated over these microstructures to trap more light inside the Si-wafer substrates. It is shown by numerous experimental and theoretical studies in the literature that textured surfaces with micro/nanostructures enhance the light trapping effect by internal reflections between the structures thus increasing the optical absorption in solar cells [24–26]. Therefore, it is expected that enhanced absorption produced on these microstructures, being the highest on the smaller feature size, will enable more efficient atomization and ionization of the analyte species and enhancements in the LIBS signal strength. However, the experimental results show that among the three structures, the substrate with larger features, CYL-20, has a better LIBS signal enhancement effect than the ones with CYL-5, and TAP-5 surfaces. This reduced signal intensity and low enhancement factors observed on triangular patterned substrates could be related to the scattering of the plasma emission, before reaching the detector, by the dust and small particles emerging from the surface after severe ablation. SEM images of the micro-structured substrate surfaces after ablation indicate a more destructive ablation occurring on the triangular patterned substrate, TAP-5, surfaces. We can also comment that the narrower spacing between 5- $\mu\text{m}$  structures may facilitate more trapping of the plasma emission signal through multiple reflections as opposed to 20- $\mu\text{m}$  ones.

Further investigations on the signal enhancement effect were

performed by comparing results from the structured, CYL-20, substrates with the non-structured, flat surfaces. The extent of magnitude in the signal enhancements with the use of structured, CYL-20, substrates relative to flat, 1000 nm and 300 nm, Si<sub>3</sub>N<sub>4</sub> coated substrates were element and emission wavelength specific. The enhancement factor of 4, for the Pb(I) 405.8 nm emission line, and 8, for the Cr(I) 428.9 nm line were observed from the CYL-20 surfaces with respect to 300 nm thick Si<sub>3</sub>N<sub>4</sub> surfaces, respectively.

This study of using microstructures on the substrate surface eliminates the problem of invisibility and inhomogeneous distribution of liquid samples on the substrate surface by defining the region where the liquid sample will be loaded. Micro-structuring substrate surfaces with an emphasis on the signal enhancement effect is also promising in terms of improvements in the signal strength and capacity of the LIBS technique via dried-droplet methodology. More research for its use in quantitative LIBS analyses is required.

### Declaration of Competing Interest

The authors declare that they have no known competing financial interests or personal relationships that could have appeared to influence the work reported in this paper.

### Data availability

No data was used for the research described in the article.

### Acknowledgments

This work was financially supported by; the Scientific and Technological Research Council of Türkiye, TUBITAK through project number 119F114 and, İYTE-BAP with project 2020İYTE004. The authors also thank Materials Research Center, MAM- İYTE for SEM images.

### References

- [1] P.J. French, P.M. Sarro, *Micromachining Technology*, in: J.G. Korvink, O. Paul (Eds.), *MEMS: A Practical Guide to Design, Analysis, and Applications*, William Andrew Publishing Inc., New York, 2006, pp. 805–853.
- [2] C.W. Ming, *Micromachining for Optical and Optoelectronic Systems*, *Proceed. IEEE* 85 (11) (1997) pp.
- [3] S. Gao, H. Huang, Recent advances in micro- and nano-machining technologies, *Front. Mech. Eng.* 12 (1) (2017) 18–32, <https://doi.org/10.1007/s11465-017-0410-9>.
- [4] Madou, M., Wang, C. *Photolithography*, in B. Bhushan, (Eds.) *Encyclopedia of Nanotechnology*, Springer, Dordrecht. (2012) pp. 2051-2060, [https://doi.org/10.1007/978-90-481-9751-4\\_342](https://doi.org/10.1007/978-90-481-9751-4_342).
- [5] Z. Huang, N. Geyer, P. Werner, J. de Boor, U. Gösele, Metal-Assisted Chemical Etching of Silicon: *Adv. Mater.* 23 (2011) 285–308, <https://doi.org/10.1002/adma.201001784>.
- [6] In-H. Song, Y.A. Peter, M. Meunier, Smoothing dry-etched microstructure sidewalls using focused ion beam milling for optical applications, *J. Micromech. Microeng.* 17 (2007) 1593–1597.
- [7] C. Oehr, H. Suhr, Deposition of silver films by plasma-enhanced chemical vapour deposition, *Appl. Phys. A* 49 (1989) 691–696.
- [8] J. Bonse, J. Krüger, S. Höhm, A. Rosenfeld, Femtosecond laser-induced periodic surface structures, *J. Laser Appl.* 24 (2012), 042006, <https://doi.org/10.2351/1.4712658>.
- [9] A.W. Miziolek, V. Palleschi, I. Schechter, *Laser-induced breakdown spectroscopy*, Cambridge University Press, 2006.
- [10] K. Keerthi, S.D. George, S.D. Kulkarni, S. Chidangil, V.K. Unnikrishnan, Elemental analysis of liquid samples by laser-induced breakdown spectroscopy (LIBS): challenges and potential experimental strategies, *Opt. Laser Technol.* 147 (2022), 107622, <https://doi.org/10.1016/j.optlastec.2021.107622>.
- [11] L.-B. Guo, D. Zhang, L.-X. Sun, S.-C. Yao, L. Zhang, Z.-Z. Wang, Q.-Q. Wang, H.-B. Ding, Y. Lu, Z.-Y. Hou, Z. Wang, Development in the application of laser-induced breakdown spectroscopy in recent years: a review, *Front. Phys.* 16 (2) (2021) 22500.
- [12] X. Wang, Y. Wei, Q. Lin, J. Zhang, Y. Duan, A. Simple, Fast matrix conversion and membrane separation method for ultrasensitive metal detection in aqueous samples by laser-induced breakdown spectroscopy, *Anal. Chem.* 87 (2015) 5577–5583.
- [13] Z. Chen, H. Li, M. Liu, R. Li, Fast and sensitive trace metal analysis in aqueous solutions by laser-induced breakdown spectroscopy using wood slice substrates, *Spectrochim. Acta B At. Spectrosc.* 63 (1) (2008) 64–68.
- [14] Q. Lin, X. Han, J. Wang, Z. Wei, K. Liu, Y. Duan, Ultra-trace metallic element detection in liquid samples using laser-induced breakdown spectroscopy based on matrix conversion and crosslinked PVA polymer membrane, *J. Anal. At. Spectrom* 31 (2016) 1622–1630.
- [15] F.J. Ruiz, L. Ripoll, M. Hidalgo, A. Canals, Dispersive micro solid-phase extraction (D $\mu$ SPE) with graphene oxide as adsorbent for sensitive elemental analysis of aqueous samples by laser-induced breakdown spectroscopy (LIBS), *Talanta* 191 (2019) 162–170.
- [16] M.A. Aguirre, S. Legnaioli, F. Almodóvar, M. Hidalgo, V. Palleschi, A. Canals, Elemental analysis by Surface-Enhanced Laser-Induced Breakdown Spectroscopy combined with liquid-liquid microextraction, *Spectrochim. Acta B At. Spectrosc.* 79–80 (2013) 88–93.
- [17] D. Zhang, A. Chen, Y. Chen, Q. Wang, S. Li, Y. Jiang, M. Jin, Influence of substrate temperature on the detection sensitivity of surface-enhanced LIBS for analysis of heavy metal elements in water, *J. Anal. At. Spectrom* 36 (2021) 1280–1286.
- [18] D. Bae, S.-H. Nam, S.-H. Han, J. Yoo, Y. Lee, Spreading a water droplet on the laser patterned silicon wafer substrate for surface-enhanced laser-induced breakdown spectroscopy, *Spectrochim. Acta B At. Spectrosc.* 113 (2015) 70–78.
- [19] A. Matsumoto, Y. Shimazu, H. Nakano, S. Yae, Signal stability of surface-enhanced laser-induced breakdown spectroscopy for microdroplet analysis using a porous silicon substrate, *Spectrochim. Acta B At. Spectrosc.* 178 (2021), 106143.
- [20] G. Yao, F. He, Q. Lin, Y. Tian, T. Zhang, B. Xu, X. Qi, Y. Duan, Synchronous detection of heavy metal ions in aqueous solution by gold nanoparticle surface-enhanced laser-induced breakdown spectroscopy, *J. Anal. At. Spectrom* 36 (12) (2021) 2639–2648.
- [21] N. Aras, Ş. Yalçın, Development, and validation of a laser-induced breakdown spectroscopic method for ultra-trace determination of Cu, Mn, Cd, and Pb metals in aqueous droplets after drying, *Talanta* 149 (2016) 53–61.
- [22] N. Aras, Ş. Yalçın, Investigating silicon wafer-based substrates for dried-droplet analysis by Laser-Induced Breakdown Spectroscopy, *Spectrochim. Acta B At. Spectrosc.* 152 (2019) 84–92.
- [23] D. Kaplan, Ş. Yalçın, Effect of silicon nitride coating thickness on silicon wafer substrates for signal enhancement in laser-induced breakdown spectroscopic analysis of liquids, *Spectrochim. Acta B At. Spectrosc.* 194 (2022), 106472.
- [24] F. Llopis, I. Tobias, Texture profile and aspect ratio influence on the front reflectance of solar cells, *J. Appl. Phys.* 100 (12) (2006), 124504.
- [25] J. Li, H. Yu, Y. Li, Optical simulation of low aspect ratio hemisphere array surface texturing for crystalline Si film solar cells, *Energy Procedia* 8 (2011) 180–184.
- [26] J. Wang, F. Zhong, H. Liu, L. Zhao, W. Wang, X. Xu, Y. Zhang, H. Yan, Influence of the textured pyramid size on the performance of silicon heterojunction solar cell, *Sol. Energy* 221 (2021) 114–119.